Electronic Supplementary Material (ESI) for Chemical Communications.
This journal is © The Royal Society of Chemistry 2020

Electronic Supplementary Information

Ultrafast, Dry Microwave Superheating for the Synthesis of SbO*x*-GNP Hybrid Anode to Investigate the Na-ion Storage compatibility in Ester and Ether Electrolyte

Sourav Ghosh[1,2], Zhimin Qi[3], Haiyan Wang[3], Surendra K. Martha[2] and Vilas G. Pol[1*]*

[1]Davidson School of Chemical Engineering, Purdue University, West Lafayette, IN 47907, USA.

[2]Department of Chemistry, Indian Institute of Technology Hyderabad, Kandi, Sangareddy, 502285, Telangana, India.

[3]Materials Engineering/Electrical and Computer Engineering, Purdue University, West Lafayette, IN 47907, USA.

*Corresponding authors. Tel: +1-7654940805; E-mail: **vpol@purdue.edu**; **martha@chy.iith.ac.in**.

S1. Experimental Section

1.1. Synthesis of SbO*x*-GNP hybrid

The synthesis of SbO*x*-GNP hybrid was carried out in a household microwave oven (Microwave Research Applications, Inc. USA). Initially, antimony acetate (Sigma-Aldrich) and graphene nanoplatelates (Sigma-Aldrich) were mixed thoroughly by maintaining the precursor's weight ratio of 10:1. The mixture was irradiated for a period of 30 seconds. Finally, the mixture was grinded to collect the SbO*x*-GNP hybrid.

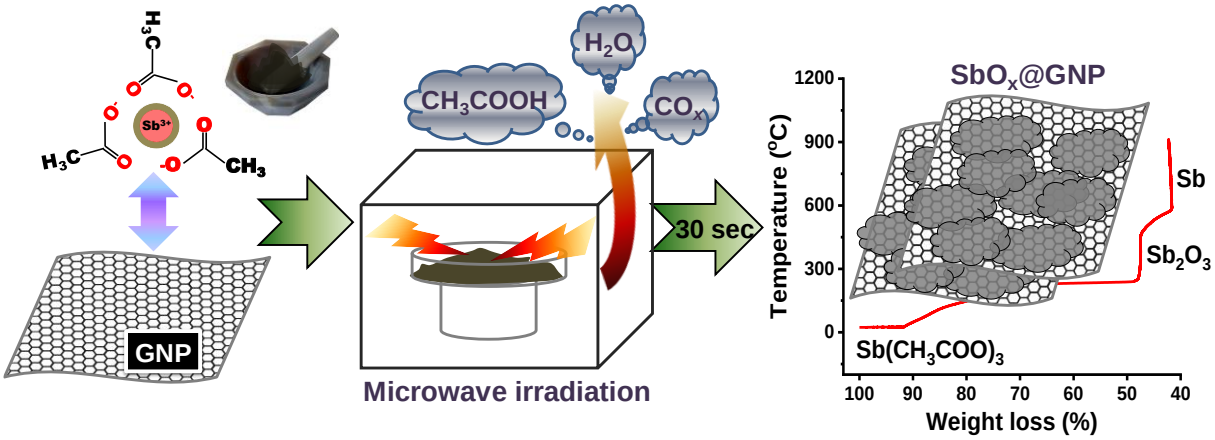

Scheme 1: Schematic representation of synthesis of SbO*x*-GNP hybrid by dry microwaving

1.2. Physical and morphological characterizations

To gain the structural knowledge of the as synthesized compound, the powder X-ray diffraction pattern was obtained by using a Rigaku SmartLab X-ray diffractometer operated at 40 kV and 40 mA with a Cu Kα radiation source (λ = 0.154 nm), between the 2θ value 10° and 80°, and the Raman Spectroscopy (Thermo Fisher Scientific DXR Raman microscope) was recorded with 633 nm laser excitation wavelength. Thermogravimetric analysis (TGA *i*-1000 instruments) was operated between the temperature ranges of 25 to 900 °C under the oxygen atmosphere, at

scan rate of 10 ^{o}C min^{-1} to calculate the GNP content in SbO*x*-GNP hybrid. Surface area of SbO*x*-GNP hybrid was evaluated by a NOVA 2200e (Quantachrome Instrments, USA) BET analyzer. The SEM and TEM images of the composite were recorded using scanning electron microscope (FEI) and transmission electron microscopy (FEI Tecnai F20 S/TEM).

1.3. Electrochemical characterizations

The anode electrode was prepared by coating the slurry on the Cu-foil current collector, followed by vacuum drying at 80 ^{o}C for 12 hours. The slurry was composed of 80% active material, 10% Super P carbon (TIMCAL Super P) and 10% PVDF (KYNAR HSV900, Arkema Inc.) as a binder in N-methyl-pyrrolidone (Sigma-Aldrich) solvent. The active material loading was controlled between 1-1.5 mg cm^{-2}. Half-cells were assembled inside the Ar-gas filled glove box (NEXUS II Vacuum Atmospheres Co.) with O_2 and H_2O level less than 1 ppm. The sodium metal foil was used as a counter electrode with GF/D (GE Healthcare Life Sciences) as the separator. The electrochemical behavior of SbO*x*-GNP anode was studied in two different electrolytic mediums- (a) Ester-based electrolyte, which was composed of 1M $NaClO_4$ in EC: PC solvent with 5% FEC (Sigma-Aldrich), and (b) Ether-based electrolyte, which was composed of 1 M $NaPF_6$ in Diglym solvent with 5% FEC. The charge-discharge cycling behavior and C-rate performance of the SbO*x*-GNP electrode was tested in the potential range between 0.01-2.5 V. The cyclic voltammetry (CV) and EIS were carried out using battery test unit model Gamry 600 potentiostat/galvanostat/ZRA. To carry out the kinetic study of SbO*x*-GNP anode, the CV at a various scan rate of 0.05, 0.1, 0.2, 0.4, 0.8, and 1 mVs^{-1} between 0.025 -2.5 V were carried out. The EIS was measured in the range of 100 MHz – 10 mHz with the voltage perturbation at 10 mV.

S2. Quantitative analysis of different Sb-phases in the hybrid using X-ray diffraction

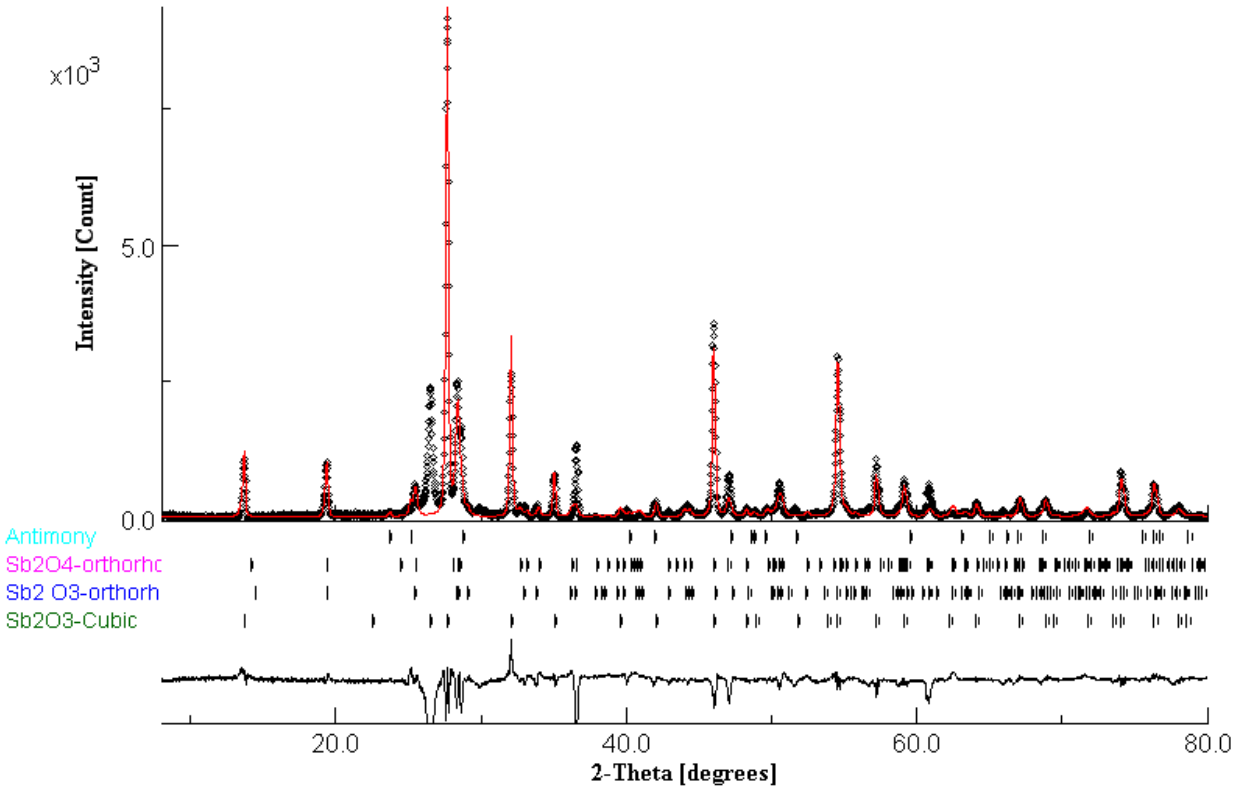

Figure S1. Refined X-ray diffraction pattern of SbOx-GNP hybrid

The refined XRD pattern suggest the presence of Sb_2O_3-cubic, Sb_2O_3-orthorhombic, Sb_2O_4-orthorhombic, and Sb-hexagonal phase with corresponding weight % of 53.7, 14.3, 30.1 and 1.9, respectively.

S3. EDS

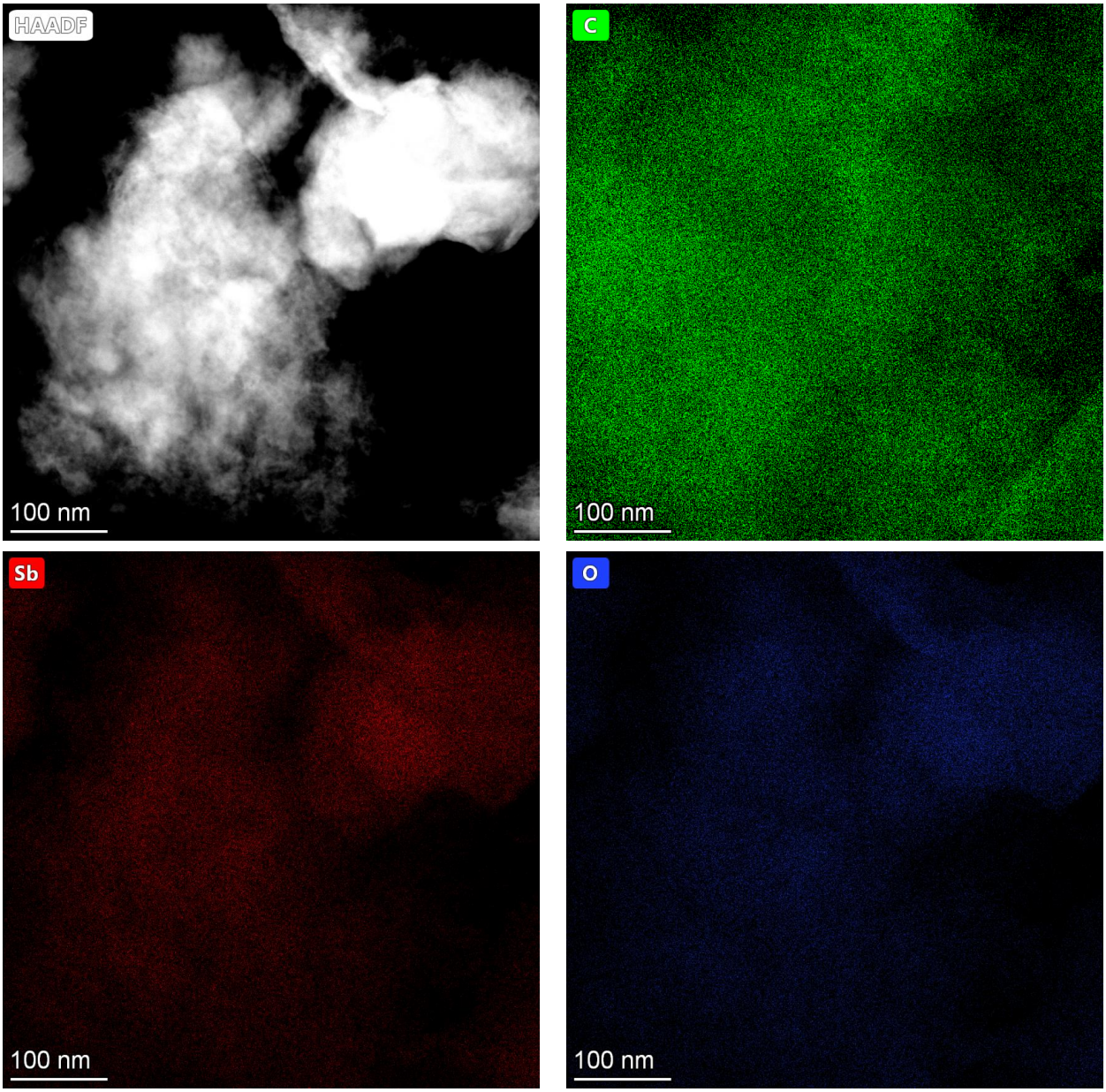

Figure S2. STEM-HAADF image and elemental mapping of SbO*x*-GNP composite.

.

S4. Characterisation of pristine GNP

The Raman spectra and TEM images of GNP are shown below. Also, HRTEM image (figure c) exhibits the lattice fringes with the d-spacing value of 0.334 nm corresponding to the (002) plan of graphitic structure. Further, in XRD pattern of the hybrid material the peak correspond to the GNP is positioned at 26.5 degree 2-theta value.

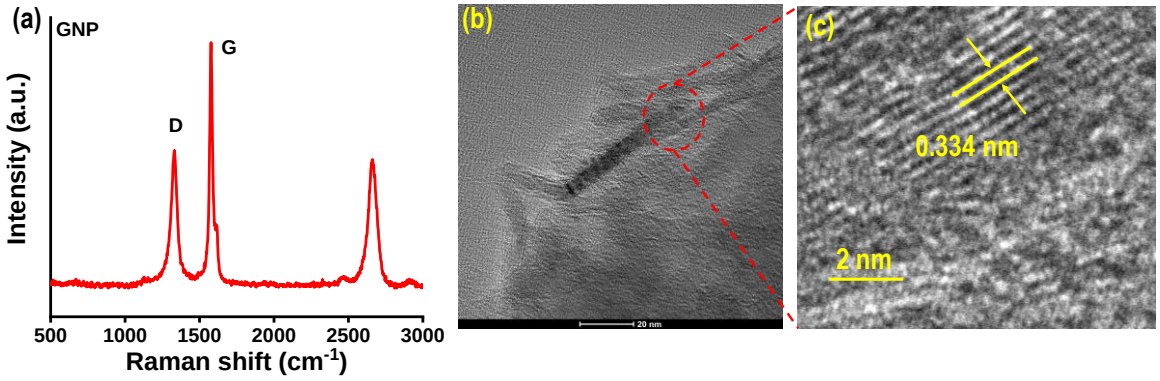

Figure S3: (a) Raman spectra; (b)-(c) TEM images of GNP

S5. dQ/dV plot

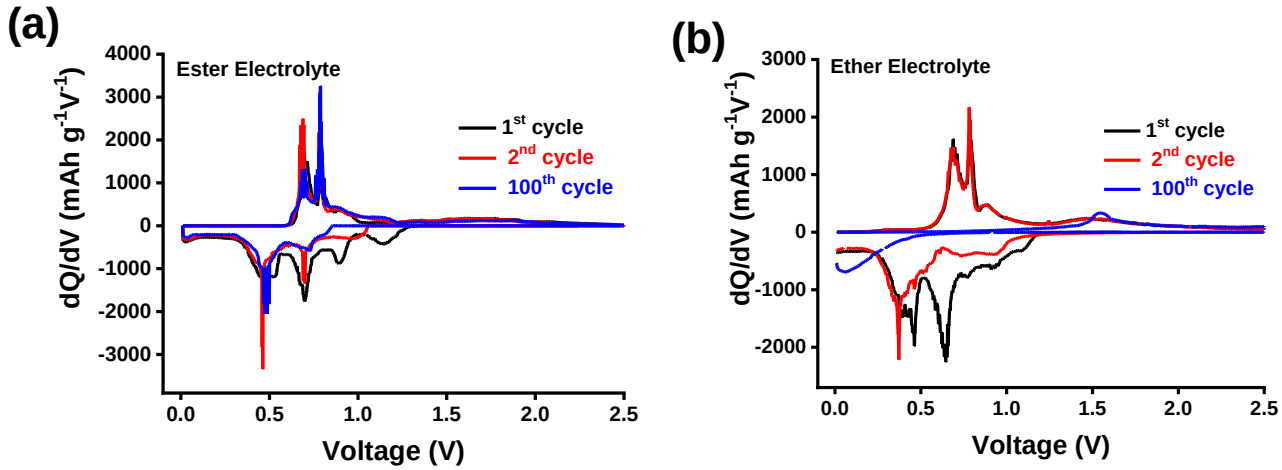

Figure S4. dQ/dV plot during 1st, 2nd, and 100th cycle in (a) Ester, and (b) Ether-based electrolytes.

S6. The electrochemical contribution of the bare GNP in both the electrolytic medium

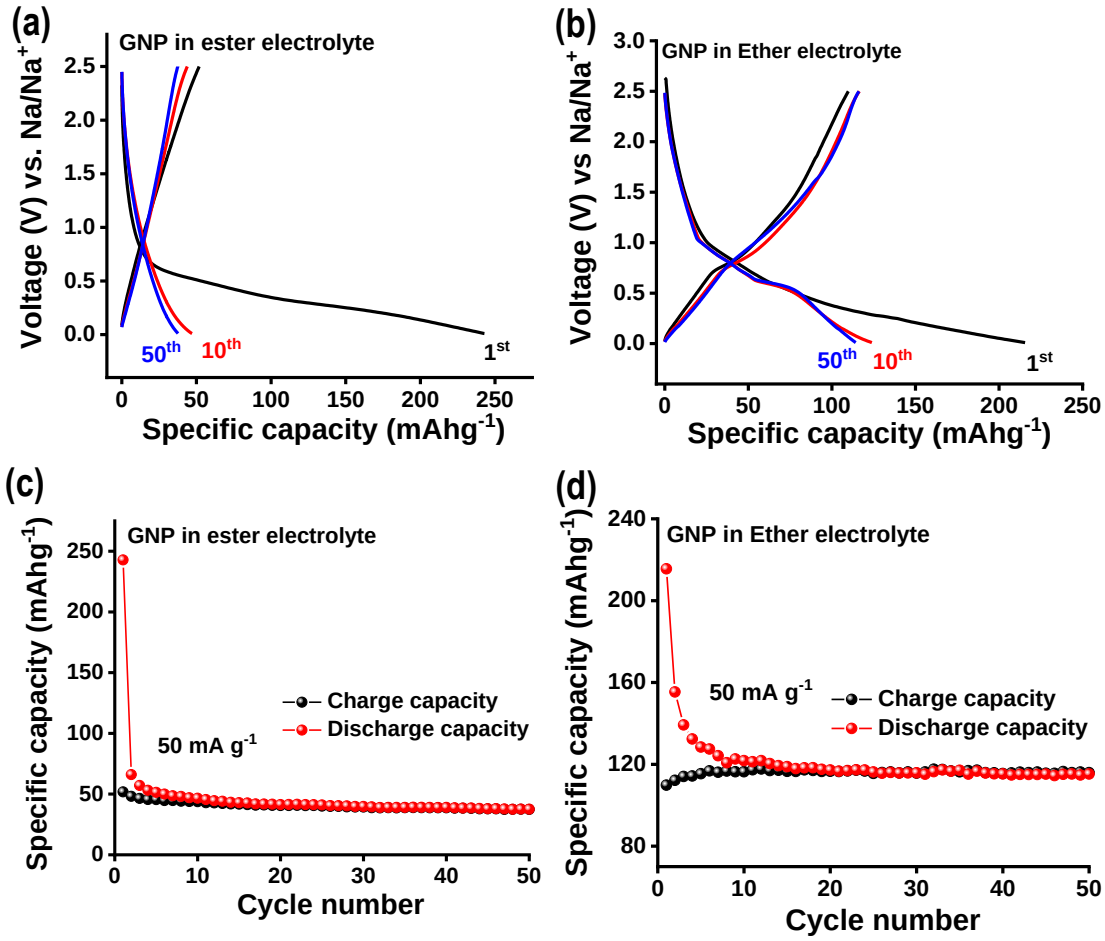

Figure S5: Charge-discharge profile of GNP in (a) Ester and (b) Ether-based electrolyte; Corresponding cycling performance in (c) Ester and (d) Ether-based electrolyte.

S7. C-rate behavior of SbOx-GNP hybrid

The C-rate performance is a crucial parameter for practical application. Figure 36 a demonstrates the rate capabilities of this anode at various current densities ranging from 100- 3000 mAg^{-1}, in ester and ether electrolytes. The corresponding charge-discharge curves at different current densities are shown in supplementary figure S6. The discharge capacity of 538 and 488 mAh g^{-1}

is observed at a lower current density of 100 and 200 mAh g^{-1}. When the current density is increased to a moderate value of 500 and 1000 mA g^{-1}, the discharge capacity decreased to 430 and 365 mAh g^{-1}. At the high currents of 2000 and 3000 mA g^{-1}, the capacity further drops to 290 and 153 mAh g^{-1}. However, in ether medium, the discharge capacity observed are 468, 410, 348, 274, 208, and 117 mAh g^{-1} at the current density of 100, 200, 500, 1000, 2000, and 3000 mAg^{-1}, respectively. After the high current test, the cell regained the capacity at low current in ester electrolyte, whereas the cell started fading in ether solvent.

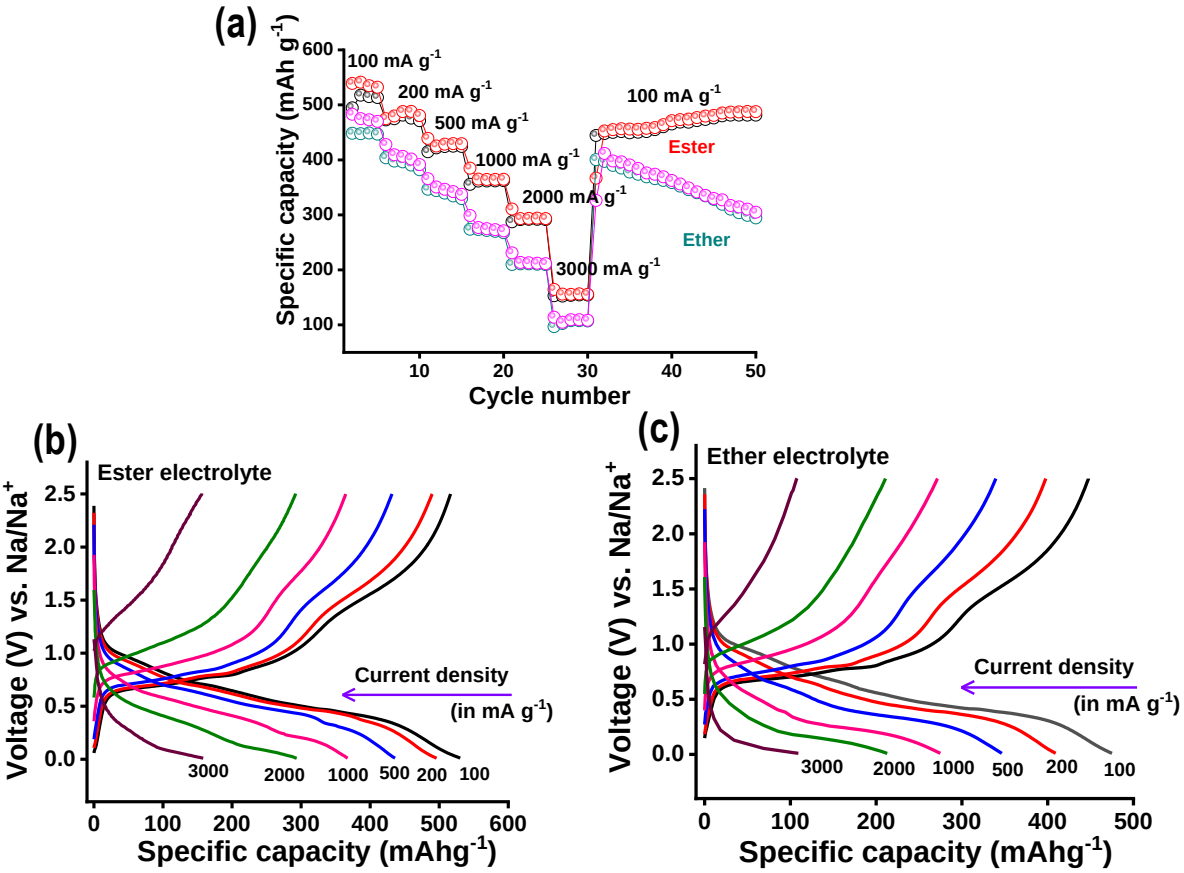

Figure S6: (a) The C-rate performance of SbOx-GNP hybrid in both the electrolytic medium; Corresponding voltage profiles at different current rates in (b) ester and (c) ether electrolytic medium

S8. Kinetic analysis of SbO*x*-GNP hybrid electrode

The overall charge storage can be quantified into diffusion-controlled Faradic process arising from conversion and alloying reaction, and capacitive-contribution from surface charge transfer according to the pioneering work of Dunn using the CV curve measured at various scan rates from 0.1 to 1 mV s^{-1} (in figure S7 a-b). Generally, the total area under the CV curve can be quantified as $Q_T = Q_C + Q_D$, where Q_T, Q_C, Q_D represents *total area* under the curve at a specific scan rate, *capacitive controlled* charge and *diffusion controlled* charge, respectively. The similar expression can be represented by following the pioneering work by Dunn et al.[1]

$$I(v) = k_1 v + k_2 v^{1/2}$$

Where, I(v), $k_1 v$ and $k_2 v$ represents the total current response, current arising from capacitive surface charge storage and current arising from diffusion controlled intercalation of Na-ion, respectively and v=scan rate. The above equation is reorganised as follows:

$$I(v)/v^{1/2} = k_1 v^{1/2} + k_2$$

In order to separate out the capacitive and diffusive component the mathematical expression is employed.

Figure S7 c-d shows the typical capacitive current contribution in comparison with the total current. At one mV s^{-1}, the capacitive contribution is observed to be 89 and 68 % in ester and ether electrolyte medium, respectively. The capacitive contribution is enhanced with the increment in scan rate from 67 % at 0.1 mV s^{-1} to 89% at one mV s^{-1} (an ester) and 35 % to 68 % in ether electrolyte under similar condition.

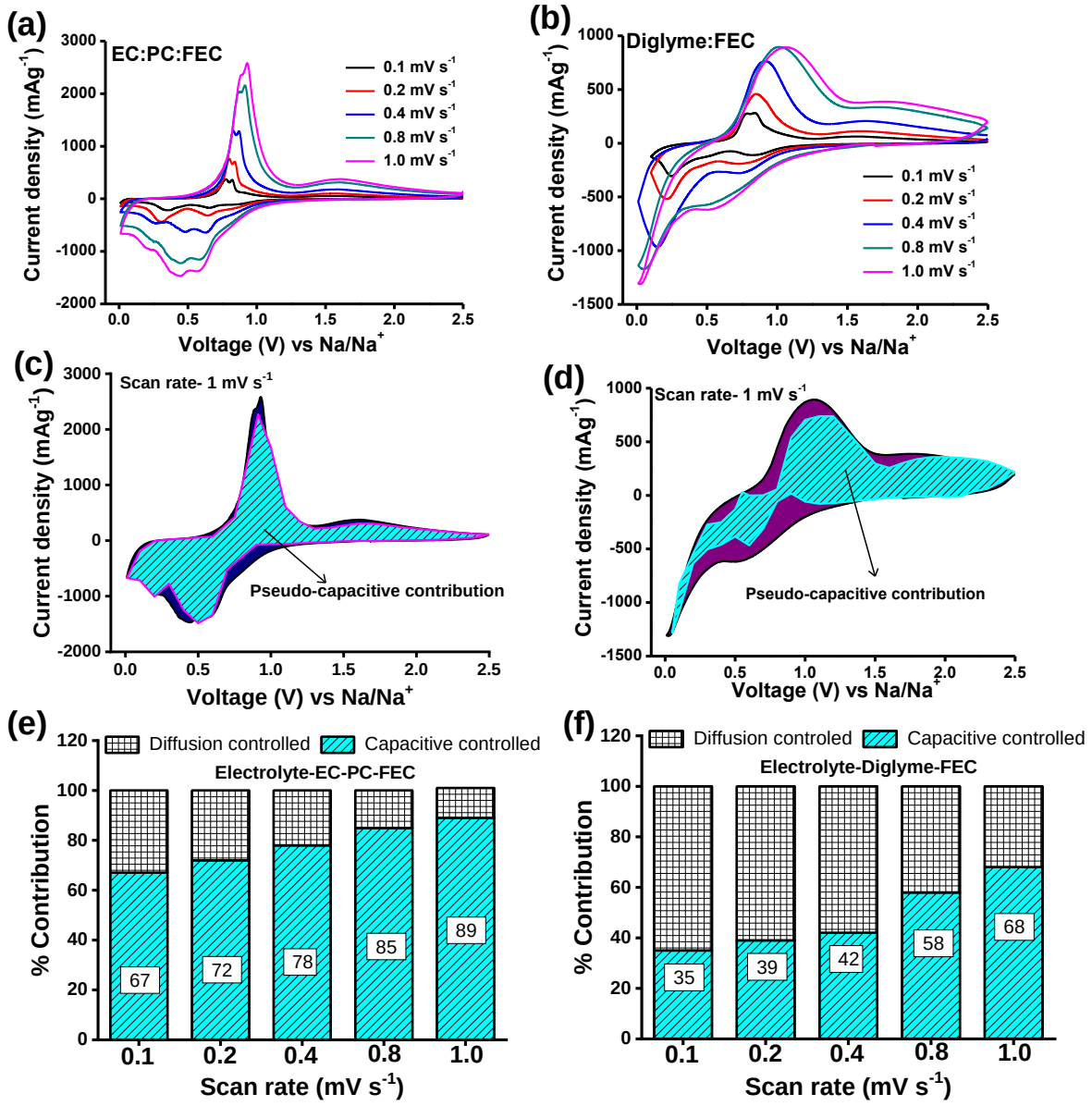

Figure S7: Cyclic Voltametry (CV) at different scan rate starting from 0.1 mV s^{-1} to 1.0 mV s^{-1} in (a) Ester and (b) Ether electrolyte; Comparison of capacitive charge storage to the overall charge storage at scan rate of 1.0 mV s^{-1} in (c) Ester and (d) Ether electrolyte; Percentage contribution from the capacitive and diffusion-controlled process at various scan rates in (e) Ester and (f) Ether electrolyte

S9. Electrochemical impedance spectroscopy (EIS) studies and further calculation of diffusion coefficient.

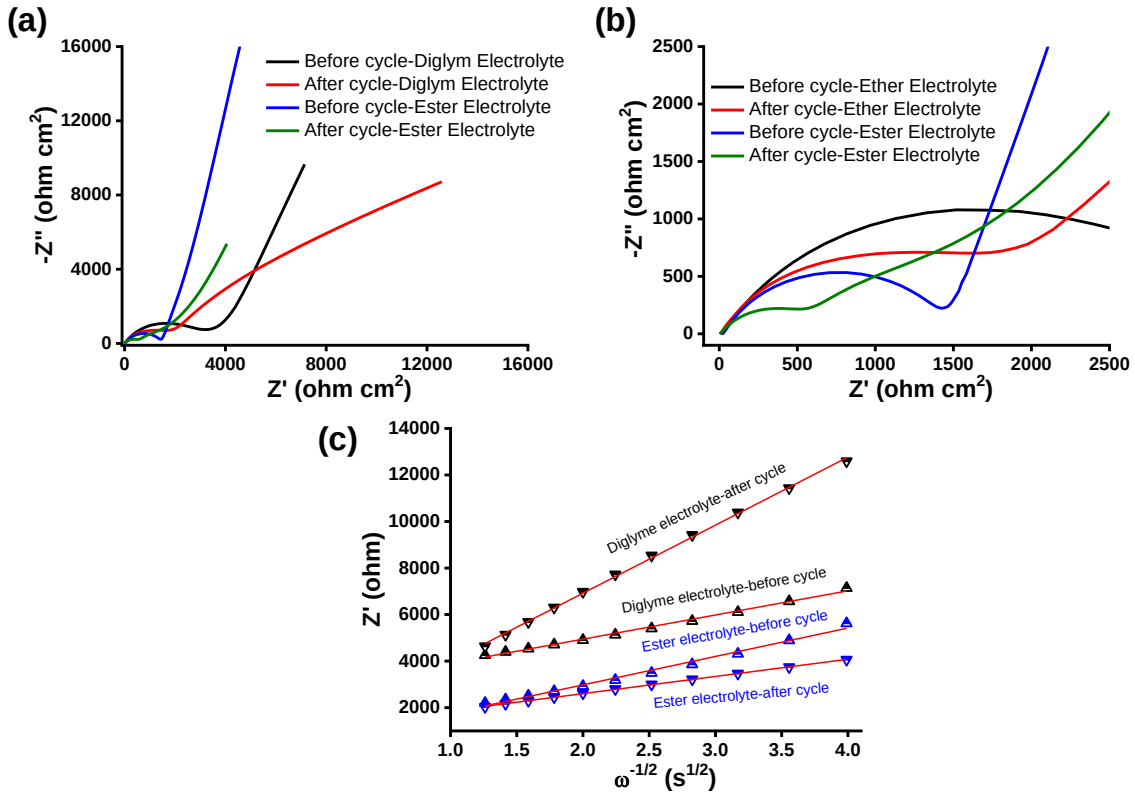

Figure S8. (a) Nyquist plot of SbO*x*-GNP electrodes before and after cycling in ester and ether electrolyte medium; (b) zoomed image of (a); (c) liner fitting of Z' vs. $\omega^{-1/2}$ to calculate Warburg coefficient.

The diffusion coefficient of sodium ion into SbO*x*-GNP electrodes in ester and ether electrolyte was calculated using following expression. [2]

$$D = \frac{0.5R^2T^2}{S^2n^4F^4c^2\sigma^2}$$

Where R is the universal gas constant (in J $mol^{-1}K^{-1}$), T is the absolute temperature (in K), S is the active surface area of the electrode (in cm^2), n is the charge transfer number, F is the Faraday's

constant (in C mol^{-1}), c is the Na-ion concentration (in mol cm^{-3}), σ is Warburg factor and D is the diffusion coefficient (cm^2 s^{-1}) measured by EIS. Warburg factor can be correlated with Z' as follows

$$Z' = R_S + R_{CT} + \sigma\omega^{-1/2}$$

Where, Z' is the real part, R_S is solution resistance, R_{CT} is charge transfer resistance, σ is wurburg factor and ω is angular frequency (=2πf). Figure S4-c represents Z' vs. $\omega^{-1/2}$ graph, which shows linear relationship and σ can be calculated from the slope of the graph. The σ value obtained here is implemented in the above mentioned diffusion coefficient and the diffusion coefficient in ester and ether based electrolyte is compared as follows-

$$\frac{D_{Na^+(ester)}}{D_{Na^+(ether)}} = \frac{\sigma_{ether}}{\sigma_{ester}}$$

Therefore, $D_{Na^+(ester)} = \left(\frac{\sigma_{ether}}{\sigma_{ester}}\right) * D_{Na^+(ether)}$

S10. FESEM images of cycled electrode

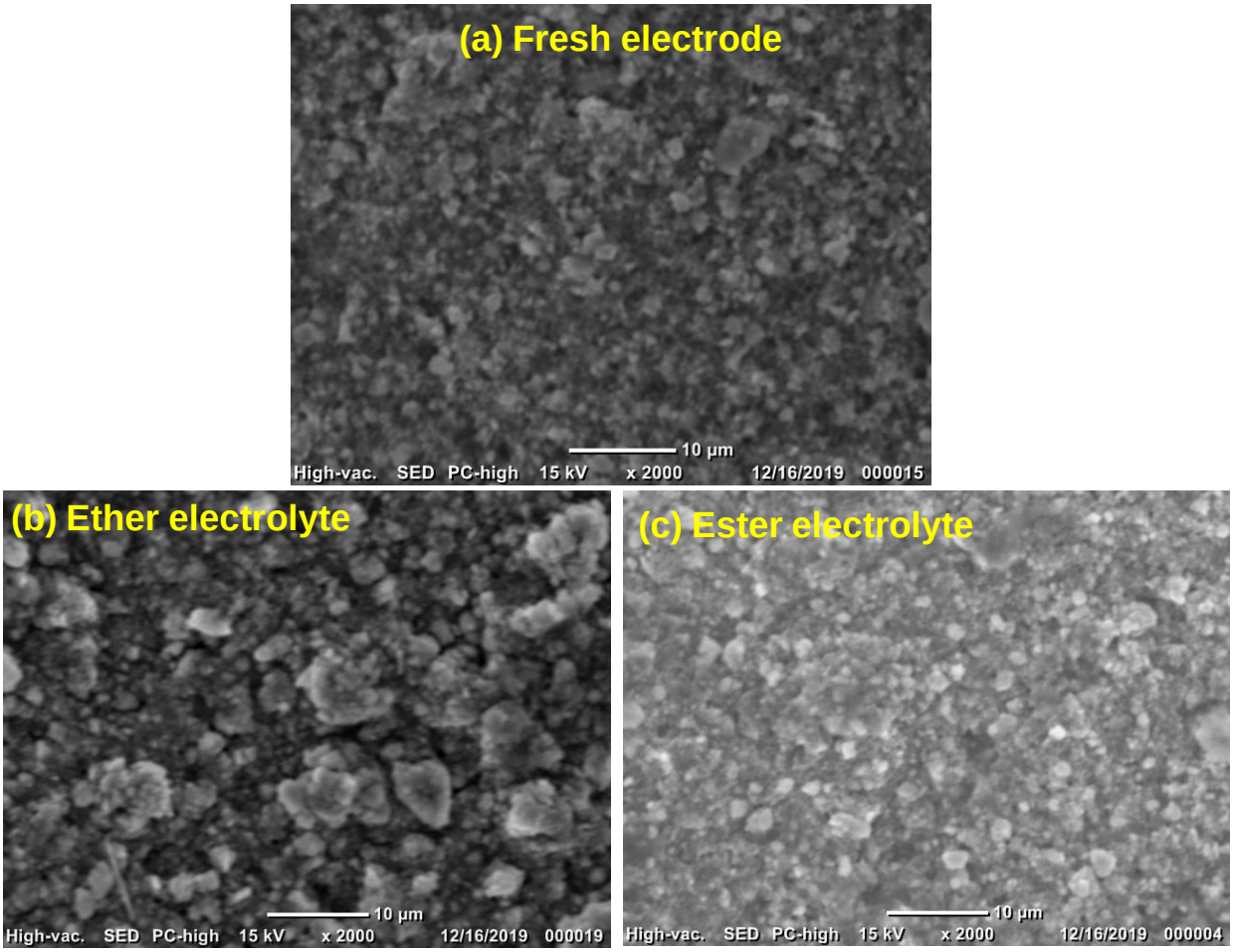

Figure S9. FESEM images of (a) fresh electrode; cycled electrode in (b) ether (c) ester-based electrolytes.

Table S1-Comparision of SbO*x*-GNP hybrid with the previously reported literature on Sb-based anode.

Materials composition	Synthetic methods (Total synthesis time)	Reversible capacity at the end of (cycle number)	Current density	Electrolyte used	Ref
Sb/Graphene nanohybrid	Solvothermal (24 hours)	211 mAh g^{-1} (30)	20 mAg^{-1}	1M $NaPF_6$ in EC:DMC	[3]
Sb/MWCNT nanocomposite	Ball-mill (12 hours)	382 mAh g^{-1} (120)	200 mAg^{-1}	1M $NaClO_4$ in EC:PC (5% FEC)	[4]
Sb nanocrystal embedded in carbon microsphere	Spray pyrolysis	372 mAh g^{-1} (100)	300 mAg^{-1}	1M $NaClO_4$ in EC:DMC (5% FEC)	[5]
Rod like Sb-C composite	Solvothermal followed by thermal annealing (40 hours)	430.9 mAh g^{-1} (100)	100 mAg^{-1}	1M $NaClO_4$ in EC:DMC	[6]
Sb@C coaxial nanotube	Hydrothermal followed by core-shell formation and thermal annealing (16 hours)	407 mAh g^{-1} (240)	100 mAg^{-1}	1M $NaClO_4$ in PC (5% FEC)	[7]
Sb/C nanocomposite	Freeze-drying followed by thermal treatment (52 hours)	372 mAh g^{-1} (100)	500 mAg^{-1}	1M $NaClO_4$ in EC:PC (5% FEC)	[8]
Sb_2O_3/Sb@graphene nanocomposites	Microwave plasma enhanced chemical vapour deposition	487 mAh g^{-1} (275)	100 mAg^{-1}	1M $NaClO_4$ in EC:DMC	[9]
SbO*x* nanoplates encapsulated by carbon flakes	Solution-evaporation followed by heat treatment (16 hr)	442 mAh g^{-1} (100)	100 mAg^{-1}	1M $NaPF_6$ in EC:DEC (5% FEC)	[10]

Self-encapsulated porous Sb–C nanocomposite	Gel formation followed by carbonisation (12 hours)	430 mAh g^{-1} (200)	1C (660 mAg^{-1})	0.6 M $NaPF_6$ in EC:DMC (3:7)	[11]
Pomegranate Sb@C yolk–shell microspheres	Solution-emulsion followed by heat treatment and HF leaching (12 hours)	600 mAh g-1 (200)	200 mAg^{-1}	1M $NaClO_4$ in EC:DMC (1:2) (10% FEC)	[12]
Porous graphene anchored with Sb/SbO*x*	Wet chemical process (Refluxing followed by reduction) (24 hours)	311.6 mAh g^{-1} (100)	50 mAg^{-1}	1M $NaClO_4$ in EC:DMC (3:7) (10% FEC)	[13]
Sb/C Fibers	Electrospinning followed by heat treatment (8 hours)	350 mAh g^{-1} (300)	100 mAg^{-1}	1M $NaClO_4$ in EC:DMC (5% FEC)	[14]
Sb Nanoparticles Encapsulated in a Reticular Amorphous Carbon Network	Electrostatic spray deposition followed by carbonisation (6 hours)	404 mAh g^{-1} (100)	0.2 C (1C=660 mAg^{-1})	1M $NaClO_4$ in EC:DEC (1% FEC)	[15]
Sb_2O_3 Film	Electrostatic spray deposition (3 hours)	414 mAh g^{-1} (200)	500 mAg^{-1}	1 M $NaPF_6$ in EC:DEC:PC (4:4:2) (5% FEC)	[16]
SbO*x*-GNP Hybrid	**Ultrafast-Dry Microwave Superheating (30 seconds)**	**481 mAh g^{-1} (100) 341 mAh g^{-1} (200)**	**100 mAg^{-1} 500 mAg^{-1}**	**1M $NaClO_4$ in EC:PC (5% FEC)**	**This Work**
		176 mAh g^{-1} (100) 48 mAh g^{-1} (200)	**100 mAg^{-1} 500 mAg^{-1}**	**1M $NaPF_6$ in Diglym (5% FEC)**	

References

[1] J. Wang, J. Polleux, J. Lim, B. Dunn, *The Journal of Physical Chemistry C* **2007**, 111, 14925.

[2] a) S. Ghosh, V. K. Kumar, S. K. Kumar, S. Biswas, S. K. Martha, *Electrochimica Acta* **2019**, 316, 69; b) W. Xu, L. Liu, H. Guo, R. Guo, C. Wang, *Electrochimica Acta* **2013**, 113, 497.

[3] Y. Zhang, J. Xie, T. Zhu, G. Cao, X. Zhao, S. Zhang, *Journal of Power Sources* **2014**, 247, 204.

[4] X. Zhou, Z. Dai, J. Bao, Y.-G. Guo, *Journal of Materials Chemistry A* **2013**, 1, 13727.

[5] Y. N. Ko, Y. C. Kang, *Chemical Communications* **2014**, 50, 12322.

[6] L. Fan, J. Zhang, J. Cui, Y. Zhu, J. Liang, L. Wang, Y. Qian, *Journal of Materials Chemistry A* **2015**, 3, 3276.

[7] Z. Liu, X.-Y. Yu, X. W. D. Lou, U. Paik, *Energy & Environmental Science* **2016**, 9, 2314.

[8] J. Duan, W. Zhang, C. Wu, Q. Fan, W. Zhang, X. Hu, Y. Huang, *Nano Energy* **2015**, 16, 479.

[9] N. Li, S. Liao, Y. Sun, H. Song, C. Wang, *Journal of Materials Chemistry A* **2015**, 3, 5820.

[10] W. Li, K. Wang, S. Cheng, K. Jiang, *Journal of Materials Chemistry A* **2017**, 5, 1160.

[11] X.-M. Pham, D. T. Ngo, H. T. Le, P. N. Didwal, R. Verma, C.-W. Min, C.-N. Park, C.-J. Park, *Nanoscale* **2018**, 10, 19399.

[12] J. Song, D. Xiao, H. Jia, G. Zhu, M. Engelhard, B. Xiao, S. Feng, D. Li, D. Reed, V. L. Sprenkle, *Nanoscale* **2019**, 11, 348.

[13] G.-Z. Wang, J.-M. Feng, L. Dong, X.-F. Li, D.-J. Li, *Journal of Alloys and Compounds* **2017**, 693, 141.

[14] Y. Zhu, X. Han, Y. Xu, Y. Liu, S. Zheng, K. Xu, L. Hu, C. Wang, *ACS nano* **2013**, 7, 6378.

[15] M. Wang, Z. Yang, J. Wang, W. Li, L. Gu, Y. Yu, *Small* **2015**, 11, 5381.

[16] M. Hu, Y. Jiang, W. Sun, H. Wang, C. Jin, M. Yan, *ACS applied materials & interfaces* **2014**, 6, 19449.